Available online at www.sciencedirect.com

SciVerse ScienceDirect

Ceramics International 38 (2012) 6009–6013

CERAMICS INTERNATIONAL

www.elsevier.com/locate/ceramint

Short communication

# Synthesis of pseudobrookite-type $Fe_2TiO_5$ nanoparticles and their Li-ion electroactivity

Kyung-Mi Min [1], Kyung-Soo Park [1], Ah-Hyeon Lim, Jae-Chan Kim, Dong-Wan Kim *

*Department of Materials Science & Engineering, Ajou University, Woncheon-dong, San 5, Yeongtong-gu, Suwon 443-749, Republic of Korea*

Received 14 February 2012; received in revised form 17 March 2012; accepted 18 March 2012
Available online 26 March 2012

**Abstract**

Phase-pure pseudobrookite $Fe_2TiO_5$ (FTO) powders with orthorhombic structures were synthesized using ball-milling (BM) and hydrothermal (HT) processes followed by thermal calcination for 2 h at 1200 and 900 °C, respectively. The morphological features and crystalline structures were characterized using field-emission scanning electron microscopy, high-resolution transmission electron microscopy, and X-ray powder diffraction. On the basis of these analyses, it was found that the calcination temperature and particle size of pure FTO could be reduced markedly when the HT method was employed. Furthermore, we have demonstrated for the first time the possibility of applying the pure FTO material as a Li-ion battery anode.



*Keywords:* Pseudobrookite $Fe_2TiO_5$; Ball milling; Hydrothermal method; Nanoparticles; Li-ion battery

## 1. Introduction

Pseudobrookite-type $Fe_2TiO_5$ (FTO) with the orthorhombic structure (space group $B_{bmm}$, $Z=4$) has typically been synthesized through conventional solid-state reactions and sol–gel methods [1–4]. In the past decade, some research groups have investigated the anisotropic spin-glass behavior and photoelectrochemical and gas-sensing properties of FTO in the form of particles, thin films, or hollow spheres [1,5–7]. However, in the case of FTO powders prepared by the solid-state reaction, there are several drawbacks such as the high formation temperature (above ≈1200 °C) and the difficulty of obtaining single-phase FTO without secondary phases [3,8]. In the case of the sol–gel process for the synthesis of FTO, almost all the research has been limited to thin films, although the temperature for the formation of FTO is lower than that required for the solid-state reaction [1,4,9].

The hydrothermal (HT) process is well known as a method for synthesizing various powders and nanostructures at low synthetic temperatures [10–15]. However, in spite of the expectation of a reduction in particle size and calcination temperature for the preparation of single-crystalline FTO, to the best of our knowledge, the HT method has not been exploited for the synthesis of pure FTO until now. In this paper, we report the synthesis of FTO powders prepared through ball-milling (BM) and HT methods, and investigate the effect of the calcination temperature on the phase transition in the samples obtained by each of these methods (BM- and HT-FTO powders). Furthermore, we demonstrate the possibility of the application of FTO as a Li-ion battery anode for the first time, as so far, there has been no study on the Li electroactivity of pure FTO materials.

## 2. Experimental procedure

### 2.1. Synthesis of $Fe_2TiO_5$ powders

*BM method*: Commercial $TiO_2$ (rutile phase, Alfa Aesar, >99%) and $Fe_2O_3$ (Alfa Aesar, 99.8%) powder mixtures with molar ratios of 1:1 and 1:0.9 were each ball-milled with $ZrO_2$ media for 48 h using absolute ethanol, and then the suspensions were dried at 90 °C in a vacuum oven. Subsequently, the homogenized mixtures were calcined at 900–1300 °C for 2 h.

*HT method*: $TiCl_3$ (7.5 mmol, Kanto, aqueous solution of ≈20%), $Fe(NO_3)_3{\cdot}9H_2O$ (15 mmol, Sigma–Aldrich, >98%),

* Corresponding author. Tel.: +82 31 219 2468; fax: +82 31 219 1612.
*E-mail address:* dwkim@ajou.ac.kr (D.-W. Kim).

[1] K.-M. Min and K.-S. Park contributed equally to this work.

0272-8842/$36.00 
doi:10.1016/j.ceramint.2012.03.044

and $NH_2CONH_2$ (37.5 mmol, Alfa Aesar, 99.3%) were dissolved in deionized water (240 mL). The pH value of the mixed solution was adjusted to 6–8 using $NH_4OH$ solution. Then, the solution was kept in a stainless steel autoclave (300 mL) at 200 °C for 48 h with stirring. The product was centrifuged, and then washed three times with deionized water and once with anhydrous ethanol. The settled powders were dried at 60 °C for 4 h in a vacuum oven. Subsequently, the obtained powders were calcined at 400–900 °C for 2 h.

### 2.2. Characterization

The morphologies and crystal structures of the prepared BM- and HT-FTO powders were analyzed by field-emission scanning electron microscopy (FE-SEM, JSM-6700F, 5 kV), high-resolution transmission electron microscopy (HR-TEM, JEM-2100F, 200 kV), and X-ray powder diffraction (XRD, Miniflex II, $\lambda_{Cu\text{-}K\alpha}$ = 1.5406 Å).

### 2.3. Electrochemical evaluation

The FTO powders were mixed in the 1-methyl-2-pyrrolidinone (NMP, Sigma–Aldrich) solvent with Super P carbon black (MMM Carbon, Brussels, Belgium) and Kynar 2801 binder (PVdF-HFP) in the mass ratio 70:15:15. For the preparation of positive electrodes, the mixture was covered evenly on Cu foil, and then dried at 100 °C for 4 h in a vacuum oven. A Swagelok-type cell was assembled in an Ar-filled glove box. This cell was composed of a positive electrode, a lithium metal foil as the negative electrode, and a separator film (Celgard 2400), which was saturated with a liquid electrolyte consisting of 1 M $LiPF_6$ dissolved in a solution of ethylene carbonate and dimethyl carbonate (1:1 by volume, Techno Semichem Co., Ltd., Korea). The fabricated cells were cycled at voltages between 3.0 and 0.01 V using an automatic battery cycler (WBCS 3000, WonaTech, Korea). Cyclic voltammograms (CVs) were measured at a scan rate of 0.1 mV $s^{-1}$.

## 3. Results and discussion

Fig. 1a shows the XRD patterns of the BM powders, in which the molar ratio of starting materials ($TiO_2$ and $Fe_2O_3$ powders) was 1:1, after calcination at various temperatures. At 900 °C, partial formation of the FTO phase was observed. As the calcination temperature of the BM powders was increased from 1000 to 1200 °C, the intensities of the peaks corresponding to the starting phases ($TiO_2$ and $Fe_2O_3$) gradually decreased, and those of the FTO phase gradually increased. When the calcination temperature was increased to 1300 °C, no reflections corresponding to the $TiO_2$ (rutile phase; JCPDS No. 21-1276) were observed, but the $Fe_2O_3$ peaks (JCPDS No. 33-0664) still remained (blue arrows in Fig. 1a). In other words, phase-pure FTO powder could not be obtained under these BM conditions, possibly because of the difficulty in the stoichiometric reaction of the $Fe_2O_3$ and $TiO_2$ powders. This result was consistent with previous reports [2]. Considering the reason for the result, the molar ratio of $Fe_2O_3$ in the starting materials was reduced to 0.9 in order to synthesize pure BM-FTO powder (using the BM process and calcination at 1200 °C for 2 h). As shown in Fig. 2, the XRD patterns of the obtained BM-FTO can be well indexed to the previously reported bulk FTO (JCPDS No. 41-1432), which has an orthorhombic structure with the space group $B_{bmm}$.

Fig. 1b shows the effect of the calcination temperature (400–900 °C) on the crystal structures of powders synthesized by the HT method. The XRD peaks of the as-prepared HT powder corresponded well to the $Fe_2O_3$ bulk material, though the peaks were broad and had low intensities because of the poor particle crystallinity and the existence of amorphous components. With calcination at 400–700 °C, the intensities of the peaks corresponding to $Fe_2O_3$ gradually increased with increasing temperature. It is noteworthy that three major peaks ($2\theta$ = 33.06°, 35.65°, and 40.85°) tended to shift toward higher $2\theta$ values as the calcination temperature was increased up to 600 °C; this effect was attributed to the substitution of $Fe^{3+}$ by

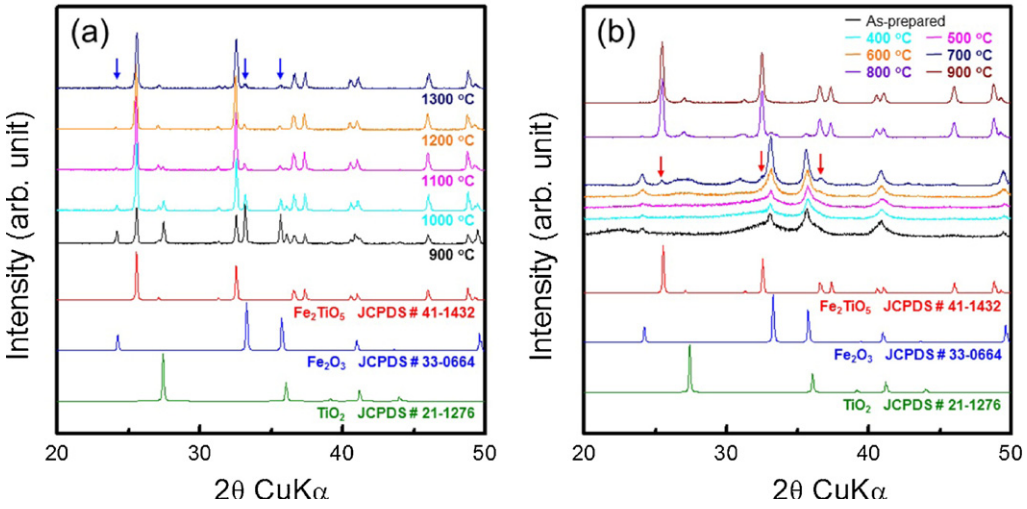


Fig. 1. XRD patterns of powders calcined at various temperatures for 2 h after (a) BM (molar ratio of 1:1) and (b) HT processes from starting mixtures containing $Fe_2O_3$ and $TiO_2$. (For interpretation of references to color in the text, the reader is referred to the web version of this article.)

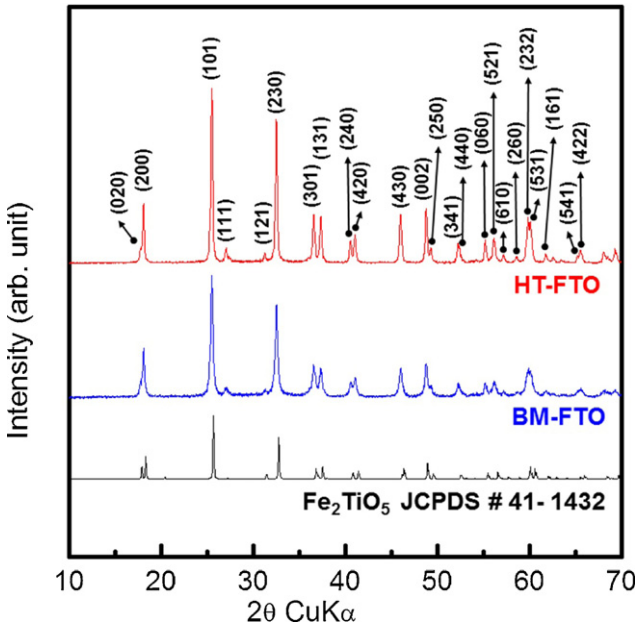


Fig. 2. XRD patterns of pure BM-FTO and HT-FTO powders obtained after calcination for 2 h at 1200 and 900 °C, respectively. The molar ratio of $Fe_2O_3$ to $TiO_2$ was 0.9 for the BM process.

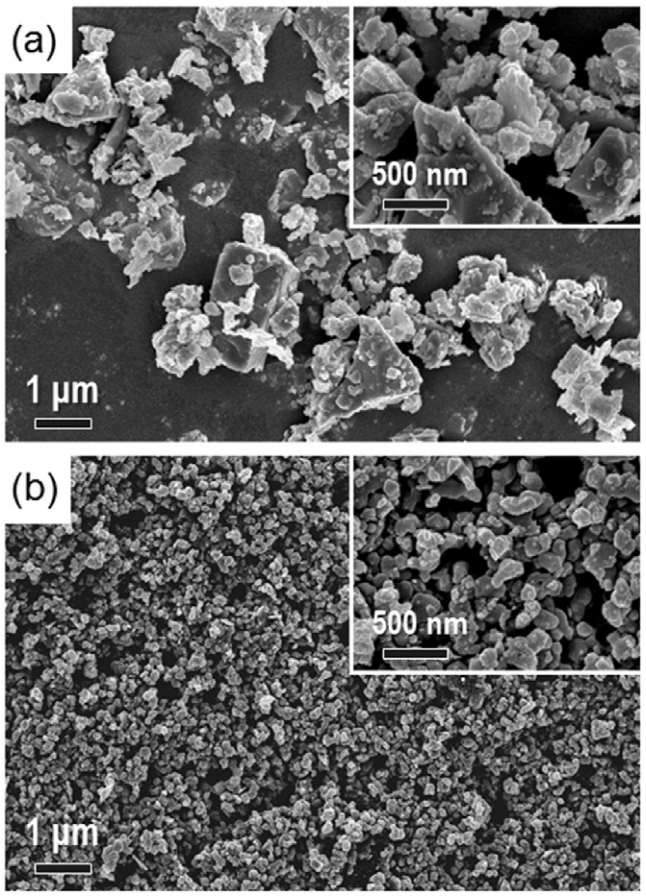


Fig. 3. Typical FE-SEM images of the (a) BM-FTO and (b) HT-FTO powders. The insets show the high-magnification FE-SEM images.

$Ti^{4+}$. The ionic radii of $Fe^{3+}$ and $Ti^{4+}$ are 0.65 and 0.61 Å [16], respectively, so the substitutional incorporation of $Ti^{4+}$ ions into the $Fe_2O_3$ lattice can cause lattice contraction of $Fe_2O_3$. In contrast, the peaks at 700 °C return to the lower $2\theta$ values because of the consumption of $Ti^{4+}$ ions located in the $Fe_2O_3$ lattice to form the new HT-FTO phase (red arrows in Fig. 1b). As the calcination temperature was increased to 800 °C, the HT powder was transformed suddenly into FTO solid solution, though a small amount of $Fe_2O_3$ containing Ti co-existed with the FTO. However, perfect HT-FTO powder without any secondary phases could be obtained when the calcination temperature was elevated further to 900 °C, as shown in Fig. 1b. From these XRD data, it was found that the formation temperature of pure FTO could be decreased remarkably when the HT method was employed.

As mentioned above, the complete conversion of the starting materials to FTO powders was achieved by the BM and HT methods, and the XRD patterns of the powders were well matched to the bulk FTO material, as shown in Fig. 2. These phase-pure BM- and HT-FTO samples were subjected to morphology analysis and electrochemical evaluation. Fig. 3 shows typical FE-SEM images of the BM- and HT-FTO powders. The BM-FTO powder showed rather irregular particle sizes and shapes (Fig. 3a and its inset). On the other hand, the HT-FTO powder exhibited a narrow size distribution and sphere-like morphology, with an average diameter of 50–200 nm (Fig. 3b and its inset).

The morphology and crystallinity of the BM- and HT-FTO powders were further investigated using TEM, HR-TEM, and fast Fourier transform (FFT), as shown in Fig. 4. The BM-FTO powder showed an irregular morphology (Fig. 4a). Periodic lattice fringes (Fig. 4b) gave interatomic plane distances of 0.331, 0.35, and 0.44 nm, which corresponded well to the *d*-spacings of the (1 1 1), (1 0 1), and (2 1 0) planes, respectively, of the pseudobrookite FTO structure (JCPDS No. 41-1432). This result was supported by the FFT pattern (Fig. 4c). The HT-FTO powders had roundish morphologies sizes of ≈100–200 nm (Fig. 4d); these results were consistent with the FE-SEM result. Through analysis of the periodic lattice fringes in the HR-TEM image in Fig. 4e and the FFT pattern in Fig. 4f, the lattice spacings of HT-FTO were found to be 0.186 and 0.49 nm, which agreed with those of the (0 0 2) and (2 0 0) planes, respectively, of the bulk FTO.

The Li electroactivity of the HT-FTO electrode was confirmed by cyclic voltammetry at room temperature in the range 3.0–0.01 V at a scan rate of 0.1 mV $s^{-1}$, as seen in Fig. 5. In the cathodic process, a well-defined peak in the range 1.0–0.5 V was observed; this could be regarded as electrochemical behavior according to the reaction of HT-FTO and Li ions. The other cathodic peak observed at ≈0.25 V in the first cycle might be ascribed to the formation of the solid electrolyte interface (SEI)-like layer, but this cathodic peak was not detected after the first cycle. Meanwhile, the two anodic peaks observed near 0.7 and 1.5 V signified the removal of Li ions from HT-FTO containing Li by a cathodic process. On the basis of this cyclic voltammogram, it was found that FTO can be used as the active anode material of a Li-ion battery. However, from the mechanisms for Li reactivity, including alloy/dealloy, conversion, and insertion/deinsertion, it

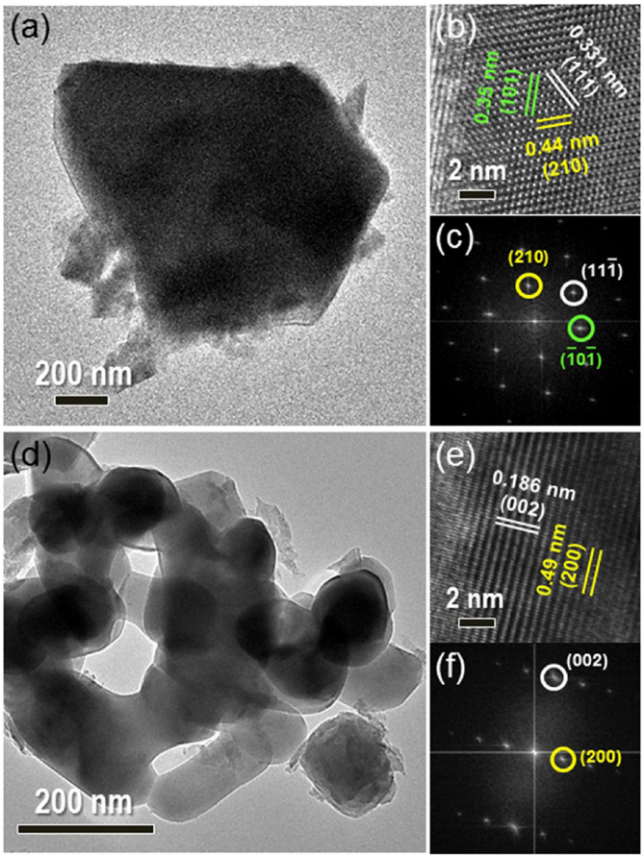


Fig. 4. Typical TEM, HR-TEM, and FFT images corresponding to the (a–c) BM-FTO and (d–f) HT-FTO powders, respectively.

is not easy to provide a clear mechanism in accordance with the FTO anode material. Additional analyses are needed to clarify the mechanism of the Li reactivity in the FTO material.

For the evaluation of the electrochemical performance of the HT-FTO electrodes, typical charge–discharge curves were recorded (Fig. 6). The cell was cycled galvanostatically at a current density of 36 mA $g^{-1}$. The specific capacity of this material in the first discharge reaction was very high (1063 mAh $g^{-1}$) and irreversible, possibly because of the formation of an SEI layer on the surface of the electrode material. In addition, this irreversible extra capacity can be attributed to the other reasons such as interfacial storage based on a capacitive behavior of the $Li_2O$/metals (Fe or Ti), electrolyte decomposition, and active material loss by disconnection of electrical contact during Li insertion [17,18].

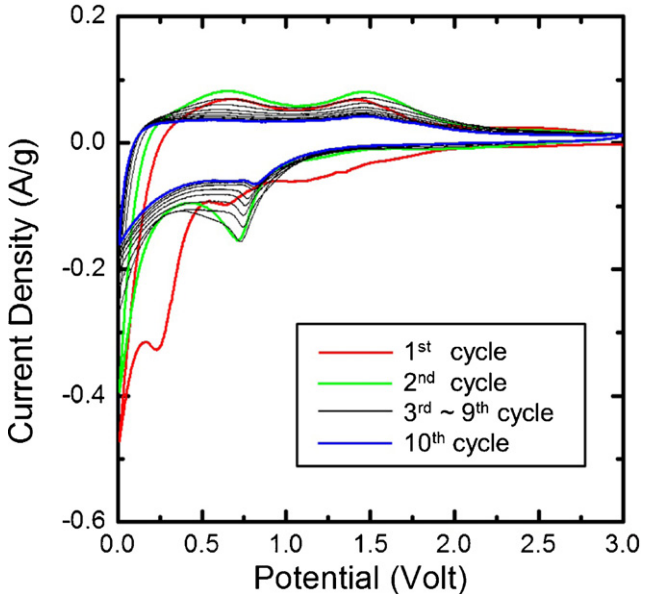


Fig. 5. Typical cyclic voltammograms of the HT-FTO powder electrode at a scan rate of 0.1 mV $s^{-1}$.

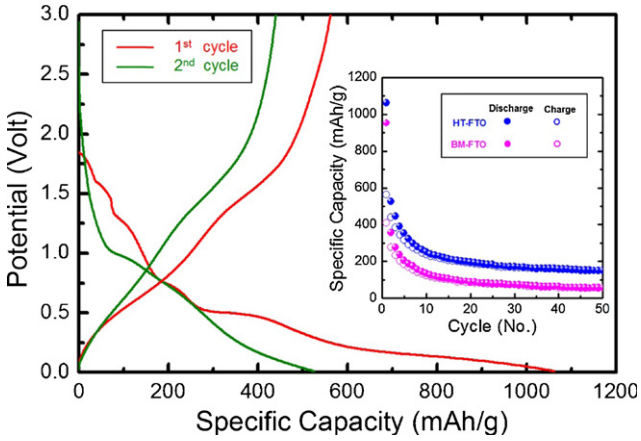


Fig. 6. Charge/discharge curves of the HT-FTO powder electrode. The inset shows the variation in the discharge/charge specific capacity versus the cycle number for the BM-FTO and HT-FTO powder electrodes.

The first charge capacity was 562 mAh $g^{-1}$. It is well known that the formation of an SEI layer consumes a large number of Li ions, leading to an increase in the irreversible capacity. The second discharge and charge capacities were 525 and 440 mAh $g^{-1}$, respectively. The specific capacities and the irreversibility between the discharge and charge capacities were stabilized after the first few cycles. The inset of Fig. 6 shows the variation of the discharge/charge capacity versus the cycle number of the pure BM- and HT-FTO electrodes at a current density of 36 mA $g^{-1}$. The reversible capacity of the BM-FTO electrode faded faster than that of the HT-FTO electrode in the initial cycles. Furthermore, the specific capacity (55.8 mAh $g^{-1}$) of the BM-FTO electrode after 50 cycles was much lower than that (151.3 mAh $g^{-1}$) of the HT-FTO electrode because of the difference in specific surface area between the two materials. In other words, a large surface area resulting from a small particle size could lead to an improvement in the specific capacity because of the larger contact area between the active material and the electrolyte.

In this work, the specific capacity of the FTO-based anode was found to be lower than that of commercial graphite (372 mAh $g^{-1}$). This might be because of an insufficient degree of electronic connection from each FTO particle to the current collector, resulting in poor capacity retention. In particular, mechanical mixing of the active FTO powder with carbon black, which is commonly used as a conducting additive, is not a proper solution for the enhancement of electrochemical properties, because the large interparticle contact resistance of FTO active materials limits the electronic conduction paths to

the current collector. Therefore, alternatives are needed to improve the electrochemical performance of the FTO-based anode, such as the formation of conducting layers (carbon and conducting polymer) on the surface of the FTO material or the incorporation of metal nanoparticles inside the FTO particles [11,19–23].

## 4. Conclusions

In summary, we have successfully synthesized highly pure pseudobrookite FTO powders with the orthorhombic structure through conventional BM and HT methods. Compared to the BM-FTO, the HT-FTO powder exhibited a smaller and more uniform particle size of ≈50–200 nm. Moreover, the calcination temperature (900 °C) for the formation of pure HT-FTO was remarkably lower than that (1200 °C) needed to obtain pure BM-FTO. Meanwhile, we have also demonstrated for the first time that FTO-based materials have the potential to be applied as new electrode materials for Li-ion batteries.

## Acknowledgement

This work was supported by the National Research Foundation of Korea (NRF) grant funded by the Korea Government (MEST) (No. 2011-005776) and Ajou University research fellowship of 2011 (S-2011-G0001-00070).

## References

[1] H. Kozuka, M. Kajimura, Sol–gel preparation and photoelectrochemical properties of $Fe_2TiO_5$ thin films, J. Sol–Gel Sci. Technol. 22 (2001) 125.
[2] M. Dondi, F. Matteucci, G. Cruciani, G. Gasparotto, D.M. Tobaldi, Pseudobrookite ceramic pigments: crystal structural, optical and technological properties, Solid State Sci. 9 (2007) 362.
[3] W.Q. Guo, S. Malus, D.H. Ryan, Z. Altounian, Crystal structure and cation distributions in the $FeTiO_5$–$Fe_2TiO_5$ solid solution series, J. Phys. Condens. Matter. 11 (1999) 6337.
[4] A.R. Phani, S. Santucci, Structural characterization of iron titanium oxide synthesized by sol–gel spin-coating technique, Mater. Lett. 50 (2001) 240.
[5] J.L. Tholence, Y. Yeshurun, B. Wanklyn, Low-temperature study of the susceptibility in the anisotropic spin glass $Fe_2TiO_5$, Solid State Phys. 19 (1986) 235.
[6] U. Atzmony, E. Gurewitz, M. Melamud, H. Pinto, Anisotropic spin-glass behavior in $Fe_2TiO_5$, Phys. Rev. Lett. 43 (1979) 782.
[7] R. Yu, Z. Li, D. Wang, X. Lai, C. Xing, M. Yang, X. Xing, $Fe_2TiO_5$/α-$Fe_2O_3$ nanocomposite hollow spheres with enhanced gas-sensing properties, Scripta Mater. 63 (2010) 155.
[8] N.I. Aljuraide, M.A.A. Mousa, M. Hessien, M. Qhatani, A. Ashour, H.L. Wamocha, H.H. Hamdeh, M.A. Ahmed, Structural properties of ferric pseudobrookite $Fe_2Ti_1O_5$ powder prepared by a new method, Int. J. Nanopart. 4 (2011) 2.
[9] A.R. Phani, F. Ruggieri, M. Passacantando, S. Santucci, Low temperature growth of nanocrystalline $Fe_2TiO_5$ perovskite thin films by sol–gel process assisted by microwave irradiation, Ceram. Int. 34 (2008) 205.
[10] I.S. Cho, S.W. Lee, J.H. Noh, D.W. Kim, D.K. Lee, H.S. Jung, D.W. Kim, K.S. Hong, $SrNb_2O_6$ nanotubes with enhanced photocatalytic activity, J. Mater. Chem. 20 (2010) 3979.
[11] G.H. Lee, J.G. Park, Y.M. Sung, K.Y. Chung, W.I. Cho, D.W. Kim, Enhanced cycling performance of an $Fe^0$/$Fe_3O_4$ nanocomposite electrode for lithium-ion batteries, Nanotechnology 20 (2009) 295205.
[12] S. Verma, P.A. Joy, Y.B. Khollam, H.S. Potdar, S.B. Deshpande, Synthesis of nanosized $MgFe_2O_4$ powders by microwave hydrothermal method, Mater. Lett. 58 (2004) 1092.
[13] H. Xu, L. Gao, J. Guo, Preparation and characterizations of tetragonal barium titanate powders by hydrothermal method, J. Eur. Ceram. Soc. 22 (2002) 1163.
[14] H.W. Shim, D.K. Lee, I.S. Cho, K.S. Hong, D.W. Kim, Facile hydrothermal synthesis of porous $TiO_2$ nanowire electrodes with high-rate capability for Li ion batteries, Nanotechnology 21 (2010) 255706.
[15] S.T. Aruna, S. Tirosh, A. Zaban, Nanosize rutile titania particle synthesis via a hydrothermal method without mineralizers, J. Mater. Chem. 10 (2000) 2388.
[16] R.D. Shannon, C.T. Prewitt, Effective ionic radii in oxides and fluorides, Acta Crystallogr. Sect. B 25 (1969) 925.
[17] S. Grugeon, S. Laruelle, L. Dupont, J.M. Tarascon, An update on the reactivity of nanoparticles Co-based compounds towards Li, Solid State Sci. 5 (2003) 895.
[18] P. Balaya, H. Li, L. Kienle, J. Maier, Fully reversible homogeneous and heterogeneous Li storage in $RuO_2$ with high capacity, Adv. Funct. Mater. 13 (2003) 621.
[19] M.S. Park, Y.M. Kang, J.H. Kim, G.X. Wang, S.X. Dou, H.K. Liu, Effects of low-temperature carbon encapsulation on the electrochemical performance of $SnO_2$ nanopowders, Carbon 46 (2008) 35.
[20] T. Zhang, L. Fu, J. Gao, L. Yang, Y. Wu, H. Wu, Core–shell Si/C nanocomposite as anode material for lithium ion batteries, Pure Appl. Chem. 78 (2006) 1889.
[21] K.S. Park, S.D. Seo, Y.H. Jin, S.H. Lee, H.W. Shim, D.H. Lee, D.W. Kim, Synthesis of cuprous oxide nanocomposite electrodes by room-temperature chemical partial reduction, Dalton Trans. 40 (2011) 9498.
[22] L. Yuan, J. Wang, S.Y. Chew, J. Chen, Z.P. Guo, L. Zhao, K. Konstantinov, H.K. Liu, Synthesis and characterization of $SnO_2$–polypyrrole composite for lithium-ion battery, J. Power Sources 174 (2007) 1183.
[23] H. Wang, Y. Zeng, K. Huang, S. Liu, L. Chen, Improvement of cycle performance of lithium ion cell $LiMn_2O_4$/$Li_xV_2O_5$ with aqueous solution electrolyte by polypyrrole coating on anode, Electrochim. Acta 52 (2007) 5102.